ELSEVIER

Polymer 42 (2001) 6609–6618

polymer

www.elsevier.nl/locate/polymer

Blends of single-site linear and branched polyethylene. II. Morphology characterisation

Bjørn Steinar Tanem[a,*], Aage Stori[b,1]

[a]Department of Machine Design and Materials Technology, Norwegian University of Science and Technology, Rich. Birkelands vei 2b, N-7491 Trondheim, Norway

[b]Department of Polymer and Composites, SINTEF Materials Technology, Forskningsveien 1, P.O. Box 124, Blindern, N-0314 Oslo, Norway

Received 24 October 2000; accepted 1 February 2001

Abstract

In this work, the morphology of a low-molecular weight single-site based linear polyethylene and several high molecular weight single-site ethylene–hexene copolymers, as well as their blends are investigated in the solid state using differential scanning calorimetry, transmission electron microscopy, atomic force microscopy and optical microscopy. Such model blends are believed to be important to elucidate the structure of polyethylene with a bimodal molecular weight distribution. The lamellae- and spherulite structure in the blend components and in the blends, and the ability to cocrystallise from the melt are found to be highly dependent on the amount of comonomer incorporation in the branched blend component. © 2001 Elsevier Science Ltd. All rights reserved.

Keywords: Ethylene–hexene copolymers; Single-site catalysts; Morphology

1. Introduction

Linear low-density polyethylene (LLDPE) represents a relatively new class of materials that entered the commercial market in the early 1980s. These materials were developed in order to produce a polyethylene with short chain branches, without any long chain branches. These materials are available in a range of densities from 0.900 to approximately 0.935 g cm^{-3}, depending on the amount of comonomer incorporated, usually 1-butene, 1-hexene or 1-octene. The market for LLDPE has increased significantly compared to low-density polyethylene (LDPE) due to high toughness, impact strength, tensile strength, elongation at strength and puncture resistance compared to LDPE-materials [1]. These materials also show an improved resistance to environmental stress cracking. However, it is known that ordinary Ziegler–Natta based LLDPE contains a considerable structural heterogeneity, with substantial amounts of the polymer having either low or high degree of comonomer incorporated [2–10]. These materials therefore show a range of properties, i.e. the low-branched fractions contribute to crystallinity, which reduces flexibility, control of melting point and clarity, while the more branched molecules contribute to surface stickiness and solubility. Furthermore, these materials show a rather broad molecular weight distribution (MWD). The low-molecular weight fractions involve extractable materials and problems with stickiness in soft copolymers, while the high-molecular weight fractions are detrimental to stiffness, melting point, clarity and rate of crystallisation. The introduction of single-site catalysts has made possible to synthesise LLDPE with a more narrow distribution of comonomer along the polymer chains and narrow MWD [5]. The problems with heterogeneous comonomer incorporation and low- and high-molecular weight fraction are therefore significantly reduced.

However, even though high-molecular weight single-site LLDPEs show superior properties in several aspects, the narrow MWD involves poor processibility and higher tendency toward melt fracture compared to ordinary Ziegler–Natta based LLDPE [11]. This problem is overcome by producing an LLDPE with a bimodal MWD. Such materials show a combination of high strength and good processibility, and are produced in a dual reactor system. The low-molecular weight fraction which contains only a few branches contributes to the processibility through an inherent lubrication effect. The properties of such bimodal LLDPE are expected to be closely related to the solid-state morphology, the phase behaviour in the melt and

* Corresponding author. Fax: +47-73-59-41-29.
E-mail addresses: bjorn.s.tanem@immtek.ntnu.no (B.S. Tanem), aage.stori@matek.sintef.no (A. Stori).
[1] Fax: +47-22-06-73-50.

PII: S0032-3861(01)00108-2

the molecular structure of the blend components. However, these systems are complex, and the molecular weights, MWD, amount- and type of comonomer and compositions of the materials should both be treated as separate variables and viewed simultaneously as a complex system. Some of the complexity is overcome when LLDPE with bimodal MWD is simulated by blending a well-defined single-site low-molecular weight LPE with a single-site well-defined high-molecular weight LLDPE [12]. In a recent work [13,14], the phase behaviour in the melt was examined in several blends of a low-molecular weight LPE and different lightly branched ethylene-1-alkene copolymers. The results indicated that such blends show considerable extent of phase separation in the melt. In another work [15], LLDPEs with bimodal MWD were simulated by blending a single-site low-molecular weight LPE with several different single-site ethylene–hexene copolymers. Thermal fractionation of the ethylene–hexene copolymers showed that some structural heterogeneity was present even though the materials were synthesised by single-site catalysts. However, cocrystallisation among the blend components seemed to be more restricted in the blends compared to what is generally found in Ziegler–Natta based materials, in accordance to results published earlier [16–18] in different blend systems. The results furthermore indicated, however, that some limited degree of cocrystallisation was present in all blends.

In this work a morphology exploration of the blend components and the blends reported in Ref. [15] is presented. The solid state morphology of the blends and blend components is investigated by differential scanning calorimetry (DSC), transmission electron microscopy (TEM), optical microscopy (OM) and atomic force microscopy (AFM).

2. Experimental

Details of most of the experimental techniques used in this work are described elsewhere [13–15,18] and will only be commented briefly here.

The materials used in this work include seven different single-site ethylene–hexene copolymers, denoted LLDPE(i); $i = 1–7$ and a single-site linear polyethylene, denoted LPE. Relevant information of these samples is found in Table 1. Two of the samples, LLDPE(6) and LLDPE(7) are extracted fractions from a bimodal copolymer [14]. Weight-average molecular weight and polydispersity were determined from GPC [13], while the amount of comonomer in the branched blend components was determined from FTIR and NMR [14]. All blends were made in solution in boiling xylene in various compositions from the LPE component and each of the copolymers. A blend containing x% (by weight) of LPE and y% (by weight) of LLDPE(i) will be denoted x/y LPE/LLDPE(i). As an example, 10/90 LPE/LLDPE(1) refers to a blend containing 10% (by weight) of LPE and 90% (by weight) of LLDPE(1). After precipitation in cold methanol, filtration, drying and vacuum treatment, film was made in a hot press. As earlier described [15], reorganisation effects are found to be highly present in these blends when the cooling rates are high. To eliminate these effects and to obtain homogeneous morphology throughout the samples, a cooling rate of 1°C min^{-1} was employed. This was obtained in a Perkin–Elmer DSC 7 equipped with a water cooling unit [15].

2.1. Optical microscopy

Circular film disks were encapsulated in DSC sample pans and went through a controlled temperature scan in DSC, by heating the samples to 170°C, held for 5 min before the samples were cooled to 10°C applying a cooling rate of 1°C min^{-1}. The heating rate was 10°C min^{-1}. This low cooling rate will most probably ensure a homogeneous morphology throughout the samples. After the thermal treatment, the samples were taken out from the sample pans, and thin sections, 2 μm in thickness were obtained

Table 1
Characterisation of the single-site based materials used in this work

	M_w[a]	M_w/M_n[a]	T_m[b]	T_c[c]	Com[d]	L_c[e] [DSC]	L_c[f] [TEM]	Density[g]
LPE	26	5	132.9	121.0	–	22.6	14.6	> 970.0
LLDPE(1)	90	2.7	123.9	112.7	1.0	12.0	9.7	937.4
LLDPE(2)	150	2.2	119.0	107.6	1.7	9.80	8.8	925.1
LLDPE(3)	115	2.5	117.9	106.9	1.8	9.4	8.4	927.8
LLDPE(4)	62	3.3	115.5	105.3	2.5	8.7	7.9	928.5
LLDPE(5)	105	2.3	110.9	98.9	4.2	7.5	6.5	919.6
LLDPE(6)	85	2.2	103.0	88.9	5.7	6.1	6.0	902.3
LLDPE(7)	58	10	95.5	83.4	7.5	5.2	5.0	902.8

[a] Weight-average molecular weight (M_w) in 10^3 g mol^{-1} and polydispersity (M_w/M_n) determined from GPC.
[b] Melting point in °C as observed in DSC using a heating rate of 10°C min^{-1} after a cooling rate of 1°C min^{-1}.
[c] Crystallisation temperature in °C as observed in DSC using a cooling rate of 1°C min^{-1}.
[d] Mol% butyl branches determined from NMR and FTIR.
[e] Lamellae thickness in nm determined from DSC and Thomson–Gibbs equation.
[f] Lamellae thickness in nm determined from TEM.
[g] Density in kg m^{-3} determined from gradient column.

in a Reichert–Jung ultramicrotome operating at −120°C and equipped with new glass knives. The sections were embedded between a microscope slide and cover glass and examined in a Zeiss Optical microscope equipped with crossed polarisers.

2.2. Atomic force microscopy

Thermal treatment of samples for AFM followed a similar procedure as the samples prepared for OM (described above). However, instead of using the sections, the surface left after cutting was employed for AFM. These surfaces were etched with a mixture of sulphuric acid, orthophosphoric acid and potassium permanganate, and washed in four separate baths according to published procedures [19]. The etching times were, however, determined individually for each sample, based on examination of samples etched for times between 30 min. and 2 h. Details of AFM instrumentation are described in Ref. [13]. Band spacing in banded spherulites was measured directly from the pictures using the Nanoscope computer software.

2.3. Transmission electron microscopy

Thermal treatment of samples for TEM was performed as described above for OM and AFM. The samples were then treated in chlorsulphonic acid following the procedure introduced by Kanig [20,21]. The samples were kept in the acid for a time range of 1 to 20 days, the actual time depends on the samples, since the rate of staining of the acid decreases with increasing crystallinity of the sample [22]. Details of cutting and instrumentation are described in Ref. [13]. Lamellae thickness were evaluated directly from negatives using an ocular and a light table.

3. Results and discussion

3.1. Morphology of the blend components

DSC crystallisation exotherms of the branched blend components LLDPE(i); $i = 1$–7 are given in Fig. 1. The cooling rate applied was 1°C min^{-1}. The crystallisation peaks show a sharp leading edge characteristic of primary crystallisation and a tail into the low-temperature region, reflecting a secondary crystallisation process involving creation of thinner lamellae. However, it is observed that the crystallisation peaks are broader and extend deep into the low-temperature regime for higher comonomer incorporation. This result indicates that the comonomer incorporation is more heterogeneous in samples containing higher amount of comonomer, in accordance to results presented elsewhere [15]. Furthermore, from Fig. 1 and Table 1 it is clear that the crystallisation temperature decreases as the amount of comonomer increases.

The lamellae in the LLDPE(1) sample are found to be rather long and slightly curved and exhibit rather uniform

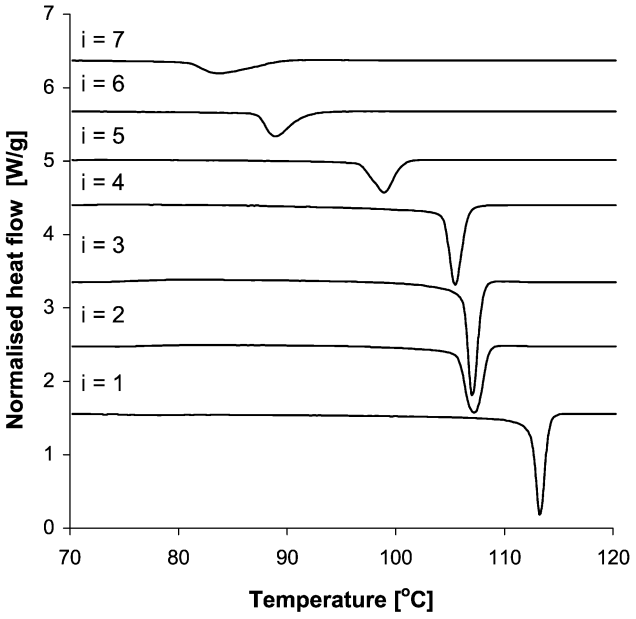

Fig. 1. DSC crystallisation exotherms of the LLDPE(i); $i = 1$–7 components used in this work. The cooling rate was 1°C min^{-1}.

thickness distribution. AFM indicates that the lamellae in this sample exhibit stacking. This is shown in Fig. 2. The most probable lamellae thickness from AFM measurements in this sample was found to be approximately 10 nm. Results from TEM furthermore demonstrate that stacking is present greatly in this sample. The most probable lamellae thickness judged from TEM was 9.7 nm, i.e. in good agreement to the AFM observations. However, it is known that shrinkage of lamellae might occur during TEM

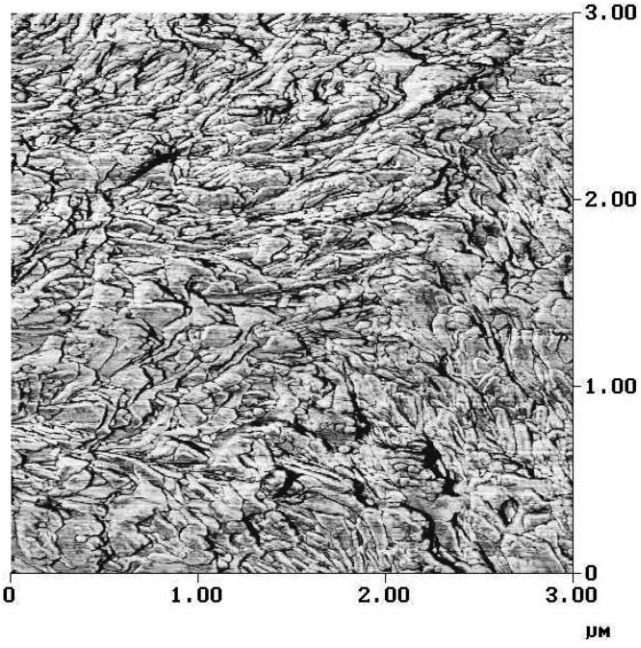

Fig. 2. AFM phase contrast of the LLDPE(1) copolymer. The sample experienced a cooling rate of 1°C min^{-1} prior to examination in AFM.

examination, due to interaction between the electron beam and polymer crystals [19,23,24]. The true lamellae thickness of the LLDPE(1) sample and the others samples examined by TEM in this work is therefore probably higher than quoted here. Furthermore, in TEM the lamellae are observed dominantly along the crystallographic *b*-axis i.e. edge on [25], which makes it much easier to measure the lamellae thickness. In AFM, the lamellae are viewed in all orientation and it is possible that the observed lamellae are not completely edge on. Results from TEM furthermore demonstrate that dominant and subsidiary lamellae are present in this sample.

A TEM picture of the LLDPE(3) blend component is shown in Fig. 3. The lamellae in the LLDPE(3) sample are found to be thinner than the lamellae observed in the LLDPE(1) sample, see Table 1. These observations are found to be general, i.e. the most probable lamellae thickness in the LLDPE(*i*) samples are found to decrease as the amount of comonomer increases. The introduction of higher amounts of branches in the polymer chains will lead to a reduced length of sequences able to crystallise with a corresponding reduction in lamellae thickness. The depression in lamellae thickness with increasing amount of comonomer incorporated is expected from the Thomson–Gibbs equation [26], which relates the lamellae thickness L_c of the samples to the melting temperature according to

$$L_c = \frac{2\sigma T_m^0}{(T_m^0 - T_m)\Delta h_f^0 \rho_c} \quad (1)$$

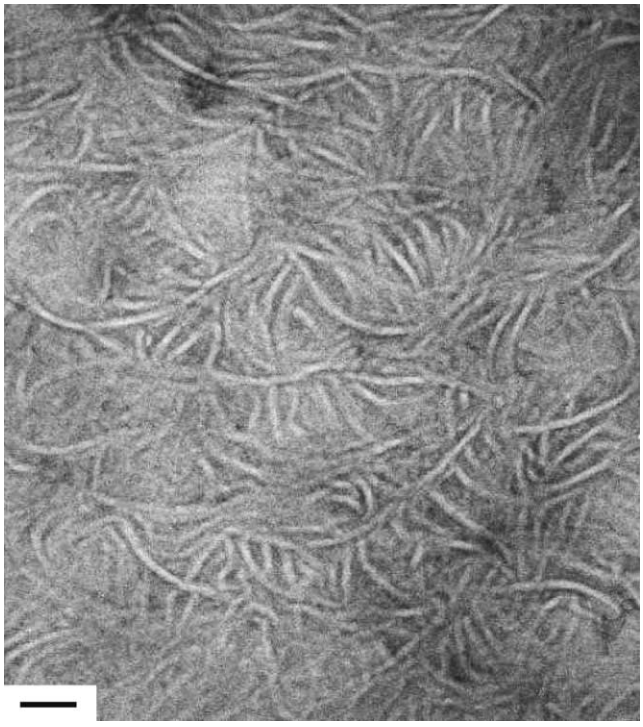

Fig. 3. TEM of the LLDPE(3) copolymer. The sample experienced a cooling rate of 1°C min^{-1} prior to examination in TEM. The scale bar in the picture is 25 nm.

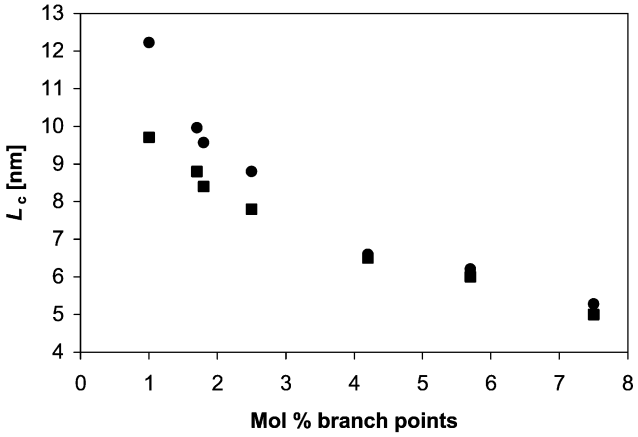

Fig. 4. Most probable lamellae thickness of the LLDPE(*i*); $i = 1$–7 components measured from TEM (■) and DSC (●) and Thomson–Gibbs Eq. (1) given as a function of the amount of comonomer incorporated.

where $\sigma = 90$ mJ m^{-2} [27] is the fold surface free energy, T_m is the melting point of the samples judged from DSC, $\Delta h_f^0 = 290$ J g^{-1} [27] is the heat of fusion for a 100% crystalline polymer at the equilibrium melting point $T_m^0 = 418.5$ K [27] and $\rho_c = 1000$ kg m^{-3} [28] is the crystal phase density. It has been pointed out that the applicability of the Thomson–Gibbs equation given in Eq. (1) is restricted for ethylene copolymers [29,30]. This is due to uncertainty in determining the surface energy and equilibrium melting temperature for ethylene copolymers. However, even though there are numerous sources of errors when lamellae thickness are calculated from Eq. (1) (surface energy and equilibrium melting temperature) and from TEM observations (shrinkage of lamellae and systematic measurement errors), the most probable lamellae thickness of the samples LLDPE(*i*); $i = 1$–7 obtained from TEM and from Eq. (1) are found to be in reasonable agreement, at least in samples where the comonomer content is higher than 2.5 mol%. This is shown in Fig. 4.

Furthermore, it is observed that the lamellae thickness distribution is broadened as the amount of comonomer increases. This is believed to support the observation from the crystallisation exotherms in Fig. 1 and results presented elsewhere [15]. In addition to the features observed in the lamellae described above, the lamellae are found to show a transition from long and straight lamellae to increasingly more curved (C-shaped) lamellae, as the amount of comonomer increases. Such curvature is believed to be associated with the tilt angle, known to be present in polyethylene [25], and plays a major role in models that seek to explain the phenomenon of banding in spherulites. The topic of banding in polyethylene spherulites is discussed in a separate paper [31].

The structure of the LPE component used in this work is found to differ somewhat from the structures of the copolymers. A TEM picture of the LPE component is shown in Fig. 5(a). Relatively long and straight occasionally roof-ridged lamellae are found to be present, in contrast to the predominantly curved C-shaped lamellae found in the

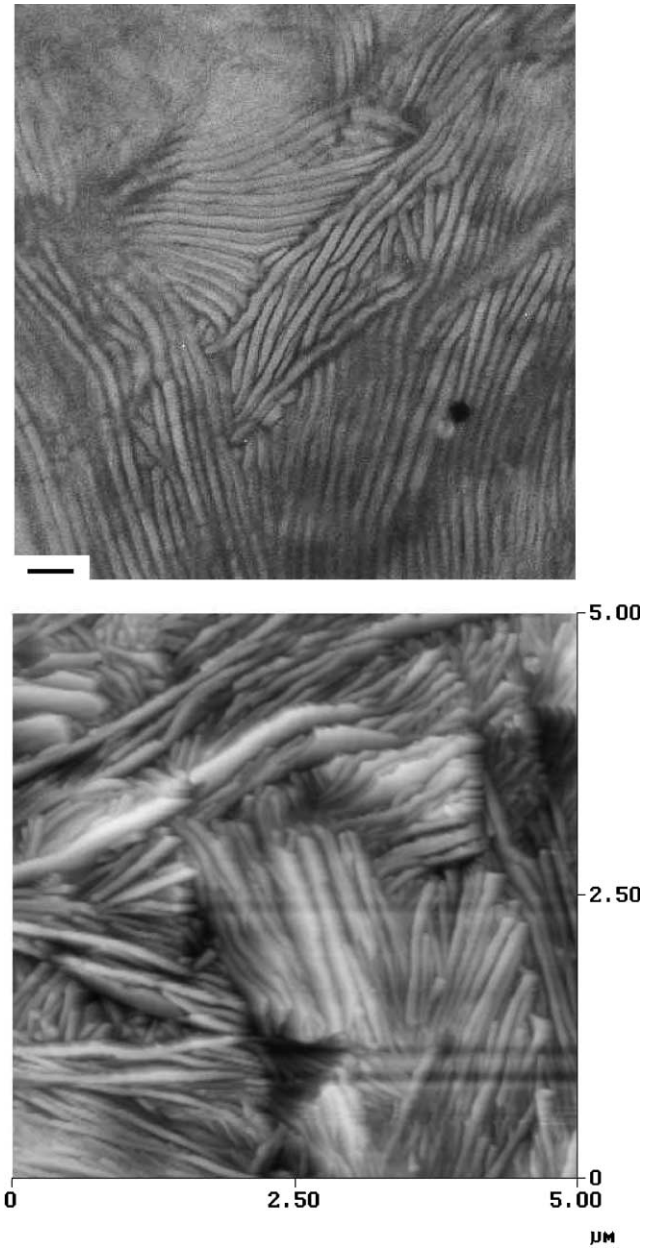

Fig. 5. (a) TEM of the LPE component. The sample experienced a cooling rate of 1°C min^{-1} prior to examination in TEM. The scale bar in the picture is 45 nm. (b) AFM topography contrast picture of the LPE component. The sample experienced a cooling rate of 1°C min^{-1} prior to examination in AFM.

LLDPE(i); $i = 1$–7 samples. The lamellae are organised in stacks, which was not the case for the branched blend components (except the LLDPE(1) sample). The most probable thickness of these lamellae, measured from TEM, is found to be 14.6 nm. Fig. 5(b) shows an AFM picture of the LPE component in topographic contrast. Lamellae stacks in all orientations are found to be present. The most probable lamellae thickness judged from AFM was found to be significantly higher than observed in TEM.

This discrepancy is probably due to the fact that the lamellae in the AFM picture in Fig. 5(b) are not viewed entirely edge on, which is done in the TEM picture in Fig. 5(a).

In the samples discussed above, the cooling rate was 1°C min^{-1}. When the cooling rate is increased, e.g. to 10°C min^{-1} the crystallisation temperatures are found to be significantly reduced. The results in Table 1 suggest that a reduction in crystallisation temperature is associated with a decrease in lamellae thickness. This result is confirmed from AFM and TEM results.

At larger scales the LLDPE(i) components exhibit a spherulite morphology. In Fig. 6(a), an AFM picture of spherulites observed in the LLDPE(1) blend component is presented. The spherulites are found to be less developed, exhibit banding and are approximately 20 μm. in diameter. When the amount of comonomer is increased e.g. in the LLDPE(3) blend component, the spherulites are found to be more developed, i.e. the number of concentric rings is increased. This is shown in Fig. 6(b), where an AFM picture of a spherulite found in the LLDPE(3) blend component is presented. The spherulite presented in Fig. 6(b) and other spherulites in the LLDPE(3) sample are found to be approximately 15–20 μm. in diameter. Lamellae radiating out from the centre of the spherulites are visible in Fig. 6(b). It is furthermore observed that the band spacing decreases as the amount of comonomer increases [31].

The spherulite structure is also found to be dependent on the cooling rate applied, i.e. spherulites are generally found to be more regular and exhibit an increasing number of concentric rings as the cooling rate is increased to 10°C min^{-1}. This observation and the morphology of the samples in Fig. 6(a) and (b) clearly demonstrate that the spherulite structure become more irregular as the crystallisation temperature increases.

An OM picture of the LPE component is shown in Fig. 7. This picture reveals that premature spherulites are present in this sample, known as axialites. This structure is generally found to be present in samples with low molecular weight and high crystallisation temperature [32–34], in agreement to the LPE sample studied here.

3.2. Morphology of the blends

It has been demonstrated elsewhere that blends, similar to the blends presented here, show extended regions of phase separation in the melt [13,14]. Based on those results it is expected that the blends 10/90 LPE/LLDPE(i); $i = 4$–7 show two separate crystal populations. The DSC crystallisation exotherms of the blends 10/90 LPE/LLDPE(i); $i = 1$–7 are given in Fig. 8. One single exotherm is found in the blends 10/90 LPE/LLDPE(1) and 10/90 LPE/LLDPE(2), indicating the formation of one single crystal population during crystallisation. However, the crystallisation exotherm in the blend 10/90 LPE/LLDPE(3) indicates the existence of a shoulder at 105°C. This is believed to indicate the existence of two crystal populations in this blend, in accordance to DSC and TEM results presented elsewhere [15].

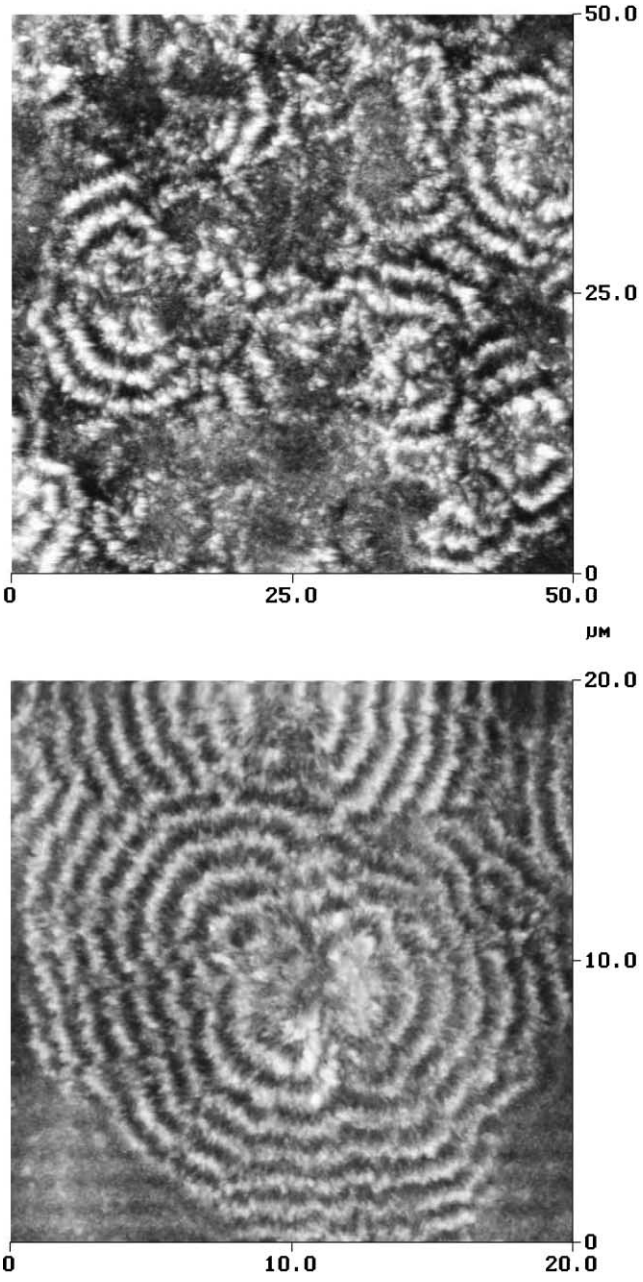

Fig. 6. (a) AFM topography contrast of the LLDPE(1) copolymer. The sample experienced a cooling rate of 1°C min^{-1} prior to examination in AFM. (b) AFM phase contrast of the LLDPE(3) blend component. The sample experienced a cooling rate of 1°C min^{-1} prior to examination in AFM.

When the amount of comonomer in the branched blend component is increased to 2.5 mol% (in the blend 10/90 LPE/LLDPE(4)), two separate crystallisation exotherms are clearly visible, indicating the formation of two crystal populations. If the amount of comonomer in the branched blend component is further increased, a better separation of the crystallisation exotherms is observed. This is shown in the blends 10/90 LPE/LLDPE(i); $i = 5$–7 in Fig. 8. Results from TEM on the blends 10/90 LPE/LLDPE(i): $i = 4$–7 clearly indicate the existence of two crystal populations in

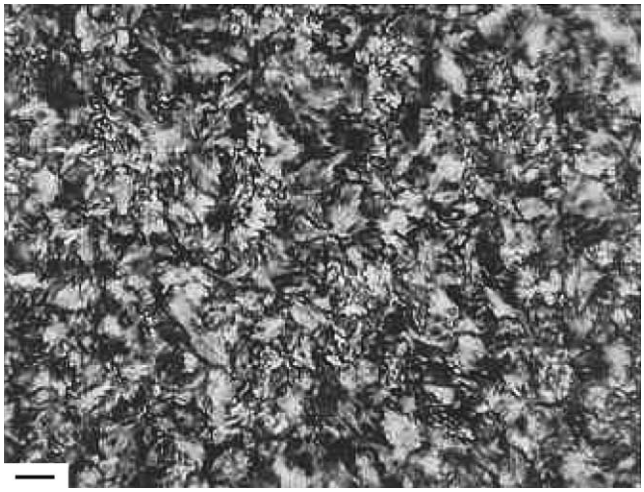

Fig. 7. OM of the LPE component. The sample experienced a cooling rate of 1°C min^{-1} prior to examination in OM. The scale bar in the picture is 10 μm.

these blends. A TEM picture of the blend 10/90 LPE/LLDPE(5) is shown in Fig. 9. A few long and relatively straight lamellae are observed in a matrix of considerable thinner lamellae that are C-shaped. The thicker lamellae are believed to correspond mainly to the LPE component in the blend, while the thinner lamellae are believed to correspond

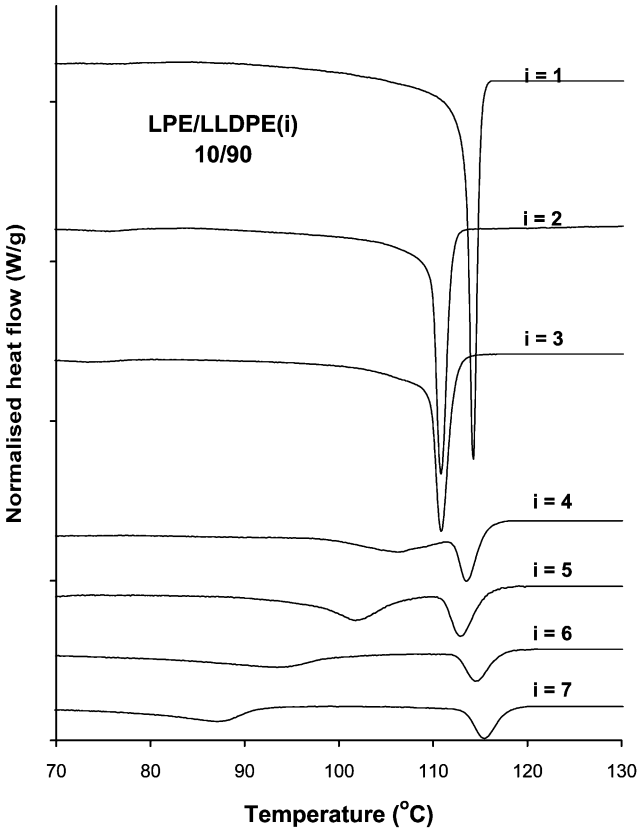

Fig. 8. DSC exotherms of the blends 10/90 LPE/LLDPE(i); $i = 1$–7. The cooling rate was 1°C min^{-1}.

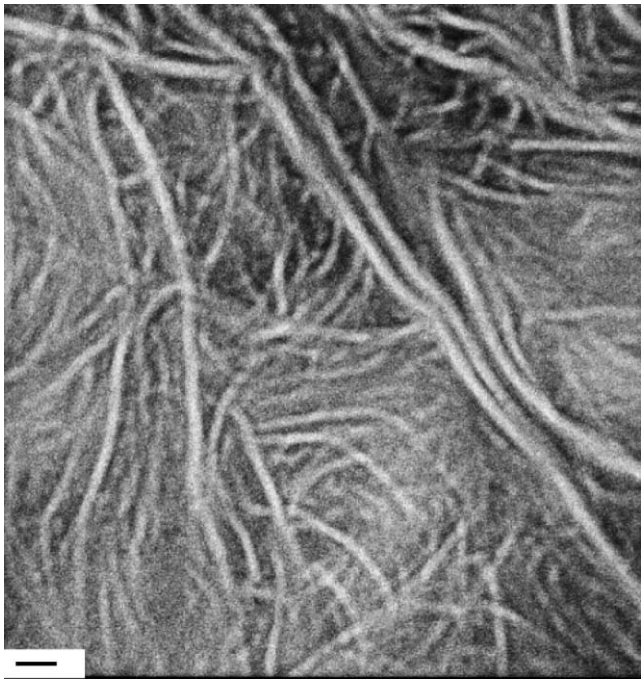

Fig. 9. TEM picture of the blend 10/90 LPE/LLDPE(5). The blend experienced a cooling rate of 1°C min^{-1} prior to examination in TEM. The scale bar in the picture is 30 nm.

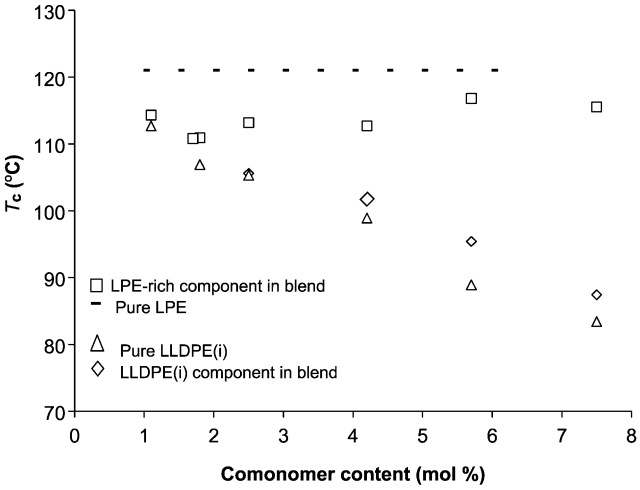

Fig. 10. Details of the blends presented in Fig. 8. The dotted lines indicate the crystallisation temperature of the pure LPE component (121°C). The rectangular boxes indicate the crystallisation temperatures of the LPE-rich components in the blends, for increasing amount of comonomer in the branched blend components. The rotated squares indicate the crystallisation temperatures of the LLDPE(*i*)-rich components in the blends for increasing amount of comonomer in the branched blend components. The triangles indicate the crystallisation temperatures of the pure branched blend components for increasing amounts of comonomer incorporated.

mainly to the LLDPE(5) component in the blend. The most probable lamellae thickness of the thicker lamellae is found to be 9.4 nm, compared to 14.6 nm in the pure LPE component. As suggested by Puig et al. [35] and discussed elsewhere [15] such depressions in lamellae thickness (together with a depression in melting- and crystallisation temperature) most probably have a complex explanation, but can be explained (at least partly) by the inclusion of some LLDPE(5) chains into the LPE lamellae during crystallisation. The thicker lamellae in Fig. 9 are therefore believed to represent an LPE-rich component. The most probable lamellae thickness of the LLDPE(5)-rich component is found to be 5.8 nm, compared to 6.5 nm in the pure LLDPE(5) component. The remaining LLDPE(5) chains, not included into the LPE-rich lamellae during crystallisation, are expected to have a higher degree of branches, and will therefore form thinner lamellae, according to the results in Table 1.

Some interesting observations of the blends shown in Fig. 8 are summarised in Fig. 10. From Fig. 10 it is observed that the crystallisation temperature of the high-temperature peak in the blends that show two crystallisation exotherms is significantly lower than the crystallisation temperature in the pure LPE component. This was observed in the 10/90 LPE/LLDPE(5) blend, as described above, and could be partly explained from the inclusion of some LLDPE(*i*) chains into the LPE lamellae during crystallisation. However, as shown in Fig. 10, a similar depression in crystallisation temperature is found in the other blends 10/90 LPE/LLDPE(*i*); $i = 4,6,7$. These results indicate that even in LLDPE(7) there exists chain segments that are able to cocrystallise with the LPE lamella during crystallisation. The results from thermal fractionation, presented in Ref. [15], indicate that such chain segments are present.

Furthermore, from Fig. 10 it is observed that the crystallisation temperature of the LLDPE(*i*)-rich component in separated blends occurs at a higher temperature than the crystallisation temperature of the corresponding pure LLDPE(*i*) components. As already pointed out, the results in this work clearly demonstrate that the lamellae thickness increases when the crystallisation temperature increases. Based on these results it is expected that the lamellae in the LLDPE(*i*)-rich components in the blends should be thicker than the lamellae in the pure LLDPE(*i*) components. However, it is demonstrated from Fig. 9 that the lamellae thickness of the LLDPE(5)-rich component in the blend is smaller than the pure LLDPE(5) component, a result found to be valid also in the blends LPE/LLDPE(*i*), $i = 4,6,7$. Moreover, in the first part of this work [15], it was concluded that the melting points of the LLDPE(*i*)-rich components in the blends occurred at *lower* temperatures than the pure LLDPE(*i*) blend components. This was explained by a limited degree of cocrystallisation among the blend components. The observation in Fig. 10, regarding crystallisation temperatures of the LLDPE(*i*) components in the blends seems therefore to be in conflict with other observations. These results will be discussed in light of observations in the blend 10/90 LPE/LLDPE(6). It has been demonstrated elsewhere that the LPE/LLDPE(6) blend system shows a wide region of phase separation in the melt phase (wide in composition and temperature) [14].

Crystallisation of the blend will therefore most probably occur from a separated melt.

In Fig. 11, crystallisation exotherms of the pure LPE component, the pure LLDPE(6) blend component and the blend 10/90 LPE/LLDPE(6) are shown. The crystallisation curves for both pure blend components show sharp leading edges, characteristic of primary crystallisation, into an axialite structure in the case of the LPE component (shown in Fig. 7) and into spherulite structure in the case of LLDPE(6). In addition, both components, especially LLDPE(6), have an extended tail to lower temperatures, reflecting a secondary crystallisation process into thinner lamellae. In the blend it is obvious from Fig. 11 that the LPE-rich component crystallises first. The crystallisation curve shows a relatively sharp leading edge for this high-temperature peak. The low-temperature peak, however, reflecting the crystallisation curve of the LLDPE(6)-rich component in the blend, do only show a broad leading edge very different from the relatively sharp crystallisation observed for the pure LLDPE(6) component. It is therefore believed that in the blend, the primary crystallisation is due to the LPE-rich component alone. The LLDPE(6)-rich component crystallises in a secondary crystallisation process within the structure determined by crystallisation of the LPE-rich component [36]. It is therefore suggested that crystallisation of the LPE-rich component will trigger the crystallisation of the LLDPE(6)-rich component at higher temperatures than the LLDPE(6)-rich component would otherwise crystallise. The lamellae thickness of the resulting LLDPE(*i*) rich components in the blends and the subsequent melting behaviour indicate that this enforced crystallisation at elevated temperature occurs without forming thicker lamellae, as normally would be expected due to higher crystallisation temperature. The blends 10/90 LPE/LLDPE(4), 10/90 LPE/LLDPE(5) and 10/90 LPE/LLDPE(7)

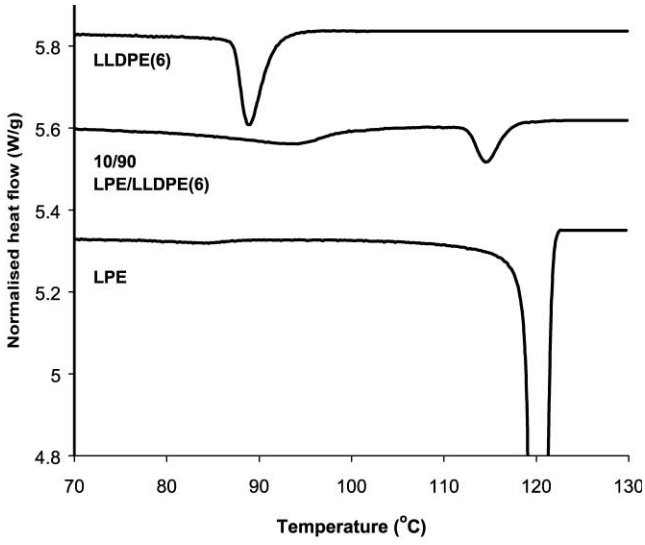

Fig. 11. DSC exotherms for the LPE component, the LLDPE(6) component and the blend 10/90 LPE/LLDPE(6). The cooling rate was 1°C min^{-1}.

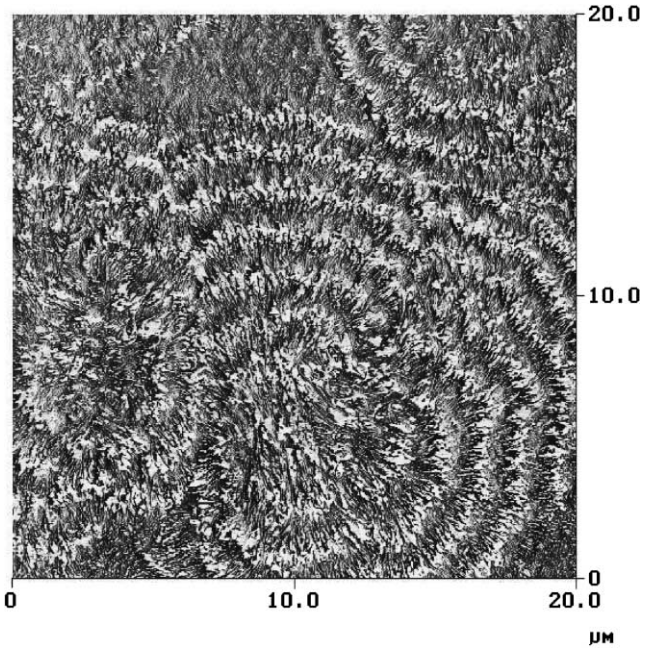

Fig. 12. AFM phase contrast of the blend 10/90 LPE/LLDPE(2). The sample experienced a cooling rate of 10°C min^{-1} prior to examination in AFM.

are found to behave similar to the blend 10/90 LPE/LLDPE(6) discussed above, and are therefore believed to show the same effect.

It is therefore clear that crystallisation of the branched blend components are highly influenced by the crystallisation of the LPE component. This is perhaps particularly clear from the AFM picture of the blend 10/90 LPE/LLDPE(2) shown in Fig. 12. In Fig. 12 it is demonstrated that two LPE axialittes are present in the centre of the spherulite (slightly below the centre in the picture) which are believed to seed the crystallisation of the LLDPE(2) component.

Furthermore, it is clear that the morphology of the blends are changed when increasing amounts of the linear blend component is added. An example of such behaviour is found when an AFM picture of the pure LLDPE(5) blend component is compared to AFM pictures of the blends 10/90 LPE/LLDPE(5) and 50/50 LPE/LLDPE(5), presented in Fig. 13(a)–(d). The AFM picture of the LLDPE(5) blend component in Fig. 13(a) clearly demonstrates that banded spherulites are found to be present, with a band spacing of approximately 0.7 μm. When 10% (by weight) of the LPE component is added, the spherulites are observed to be less regular and the band spacing is increased to approximately 3.8 μm. This is shown in an AFM picture in Fig. 13(b) and an OM picture in Fig. 13(c). The results in Fig. 13(b) and (c) demonstrate that AFM and OM are complementary techniques for the observation of large-scale structures, at least for the particular blend discussed here. However, the AFM technique is able to resolve finer details in the structure. It has been demonstrated elsewhere that AFM is able to

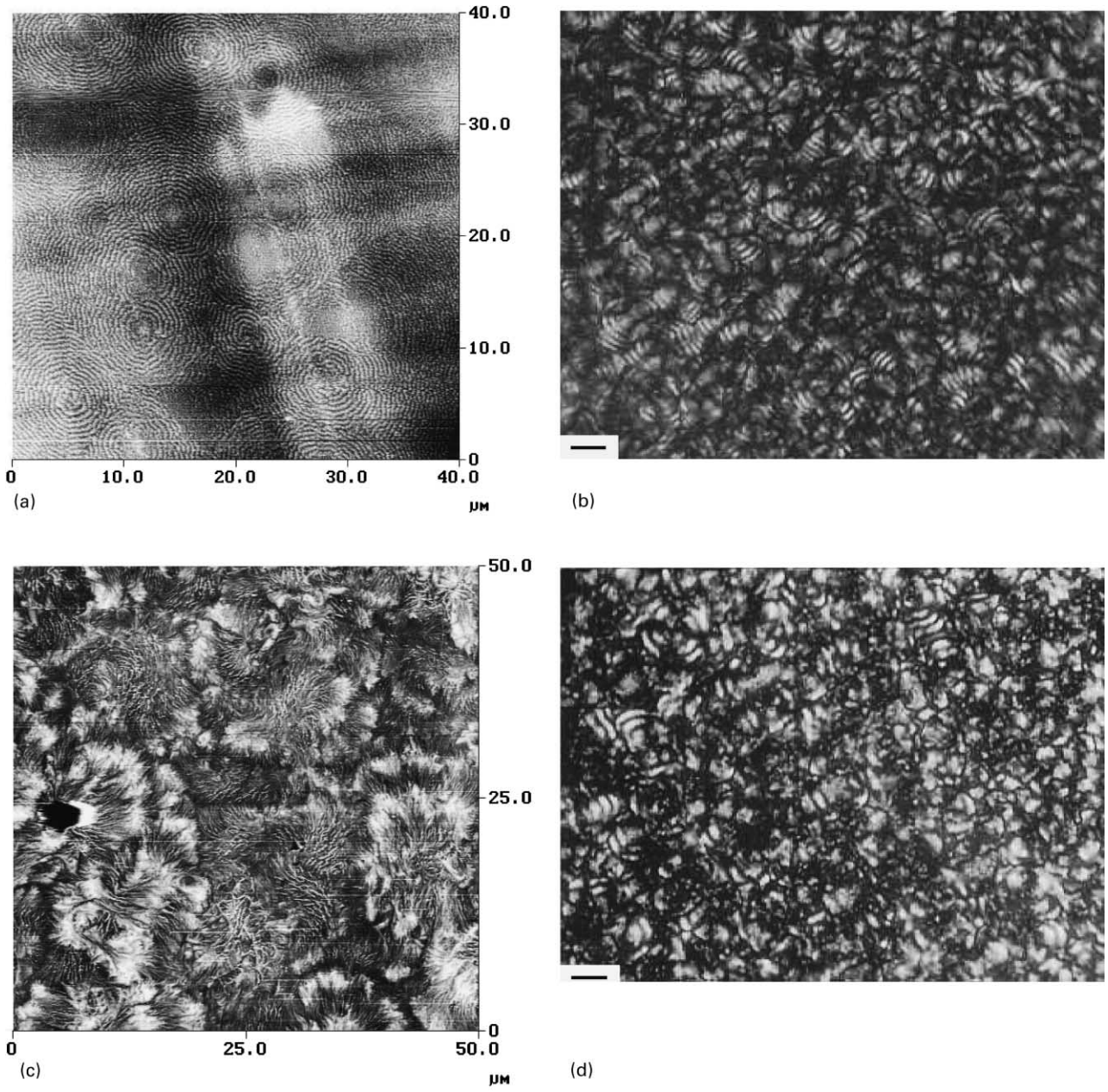

Fig. 13. (a) AFM phase contrast of the LLDPE(5) blend component. The sample experienced a cooling rate of 1°C min^{-1} prior to examination in AFM. (b) AFM phase contrast of the blend 10/90 LPE/LLDPE(5). The blend experienced a cooling rate of 1°C min^{-1} prior to examination in AFM. (c) OM of the blend 10/90 LPE/LLDPE(5). The blend experienced a cooling rate of 1°C min^{-1} prior to examination in OM. The scale bar in the picture is 15 μm. (d) OM of the blend 50/50 LPE/LLDPE(5). The blend experienced a cooling rate of 1°C min^{-1} prior to examination in OM. The scale bar in the picture is 15 μm.

resolve banding in spherulites where OM indicates the presence of non-banded structure [31]. This discrepancy is most probably due to the limited resolving capability in OM.

When the amount of the LPE component in the blend is further increased to 50% (by weight), the spherulite structure is almost completely broken down, as shown in Fig. 13(d). A few spherulites having a limited number of concentric rings are, however, visible, with a band spacing of approximately 4.5 μm. A similar morphology is observed from AFM. A further increase in the amount of the LPE component will result in a morphology where the spherulite structure is completely broken down, and is more similar to an axialite structure. These results clearly demonstrate that a transition from banded spherulites into an axialite morphology occurs as the amount of the linear blend component in the blend increases.

In two of the blend systems, LPE/LLDPE(4) and LPE/LLDPE(6) a transition from banded spherulites into non-banded spherulites (as observed in AFM) is observed when 10% by weight of the LPE component is added. By further increasing the amount the linear component in the blend, a transition from a morphology dominated by non-banded

spherulites to a morphology dominated by axialites is observed.

Furthermore, TEM results of the blends 50/50 LPE/LLDPE(i); $i = 4–7$ and 75/25 LPE/LLDPE(i); $i = 4–7$ show the existence of two separate crystal populations, in agreement to results obtained elsewhere [15].

4. Conclusions

In this work the morphology of a low-molecular single-site based linear polyethylene and several higher molecular weight single-site ethylene–hexene copolymers, as well as their blends are investigated in the solid state using DSC, TEM, OM and AFM. It is believed that these blend components as well as their blends are of fundamental importance to those concerned with structure and properties of bimodal PE systems prepared from single-site catalysts. Observations of lamellae in the copolymers demonstrate that an increase in the amount of comonomer is associated with a decrease in crystallisation temperature and lamellae thickness and a transition from rather straight long lamellae into increasingly more curved (C-shaped) and shorter lamellae. A successive broadening in the lamellae thickness distribution is also observed as the amount of comonomer increases. This is believed to indicate a more heterogeneous comonomer distribution in samples with high amounts of comonomer incorporation compared to samples with smaller amount of comonomer incorporation. Furthermore, the results obtained suggest that cocrystallisation among the blend component is limited, even 1.8 mol% comonomer in the branched blend component is believed to generate the existence of two crystal populations in the blends. This is probably due to the rather homogeneous nature of single-site materials.

In blends showing two crystal populations the crystallisation temperature of the component rich in the branched blend component is higher than that of the corresponding pure branched blend components. However, this is not accompanied with an increase in lamellae thickness. Results from TEM suggest on the contrary that the lamellae in the components rich in the branched blend component are thinner than the corresponding pure branched components. The explanation of these observations is not completely clear, however, a qualitative scheme based on a seeding effect of the LPE blend component is suggested.

The spherulite structure in the blends are found to be highly dependent on the crystallisation temperature, i.e. the spherulites are observed to be less regular with a decreasing number of concentric rings as the crystallisation temperature increases.

Acknowledgements

Financial support from the Norwegian Research Council (NFR) under the Polymer Science Program is gratefully acknowledged. The authors also want to thank Heidi Nornes Bryntesen at Borealis for GPC measurements and Irene Helland at Borealis for help with density characterisation of materials.

References

[1] Brydson JA. Plastics materials. London: Butterworths-Heinemann, 1995.
[2] Wild L, Ryle T, Knobeloch D. Am Chem Soc Polym Prepr 1982;23:133.
[3] Wild L. Adv Polym Sci 1990;98:1.
[4] Mathot VBF, Pijpers MF. J Appl Polym Sci 1990;39:979.
[5] Brintzinger HH, Fischer D, Mulhaupt R, Rieger B, Waymouth RM. Angew Chem, Int Ed Engl 1995;34:1143.
[6] Wignall GD, Alamo RG, Londono JD, Mandelkern L, Stehling FC. Macromolecules 1996;29:5332.
[7] Karbaschewski E, Kale L, Rudin A, Tchir WJ, Cook DG, Pronovost JO. J Appl Polym Sci 1992;44:425.
[8] Schoutern P, Groeninckx G, der Heijden BV, Jansen F. Polymer 1987;28:2099.
[9] Mirabella FM, Ford EA. J Polym Sci, Polym Phys Ed 1987;25:777.
[10] Mirabella FM, Westphal SP, Fernando PL, Ford EA, Williams JG. J Polym Sci 1988;B26:1995.
[11] Scheirs J, Bõhm LL, Boot JC, Leevers PS. TRIP 1996;4(12):408.
[12] Mandelkern L, Alamo RG, Wignall GD, Stehling FC. TRIP 1996;4(11):377.
[13] Tanem BS, Stori Aa. Polymer 2001;42(9):4309.
[14] Tanem BS, Stori Aa. Polymer 2001;42(13)5699.
[15] Tanem BS, Stori Aa. Polymer 2001;42(12):5393.
[16] Zhao Y, Liu S, Yang D. Macromol Chem Phys 1997;198:1427.
[17] Lee SY, Jho JY, Huh W. J Ind Engng Chem 1998;4(3):258–62.
[18] Tanem BS, Stori Aa. Thermochim Acta 2000;345:73.
[19] Patrick M, Bennett V, Hill MJ. Polymer 1996;37(24):5335.
[20] Kanig G. Kolloid Z Z Polym 1973;251:782.
[21] Kanig G. Prog Colloid Polym Sci 1975;57:176.
[22] Morgan RL, Hill MJ, Barham PJ. Polymer 1999;40:337.
[23] Hill MJ, Bradshaw DC, Chevili R. Polym Commun 1992;33:844.
[24] Grubb DT, Keller A, Groves GW. J Mater Sci 1972;7:131.
[25] Gedde UW. Polymer physics. London: Chapman & Hall, 1995.
[26] Trãnkner T, Hedenquist M, Gedde UW. Polym Engng Sci 1994;34:1581.
[27] Hoffmann JD, Miller RL, Marand H, Roitman DB. Macromolecules 1992;25:2221.
[28] Wunderlich B. Macromolecular physics: crystal structure, morphology and defects, vol. 1. New York: Academic Press, 1973.
[29] Zhou H, Wilkes GS. Polymer 1997;38(23):5735.
[30] Lu L, Alamo RG, Mandelkern L. Macromolecules 1994;27(22):6571.
[31] Tanem BS, Stori Aa, submitted for publication.
[32] Rego Lopez JM, Gedde UW. Polymer 1988;29:1037.
[33] Hoffmann JD, Frolen LJ, Ross GS, Lauritzen Jr. JI. J Res Natl Bur Stand 1977;79A:671.
[34] Maxfield J, Mandelkern L. Macromolecules 1977;10:1141.
[35] Puig CC, Hill MJ, Odell JA. Polymer 1993;34:3402.
[36] Ueda M, Register RA. J Macromol Sci Part B 1996;B35(1):23.